Detection of nucleotides adsorbed onto clay by UV resonant raman spectroscopy: A step towards the search for biosignatures on Mars

G. Montagnac, J. Hao, U. Pedreira-Segade, I. Daniel

Version of Record: https://www.sciencedirect.com/science/article/pii/S0169131720303896
Manuscript_353882524b78a788d7da044b1ccf336b

Detection of nucleotides adsorbed onto clay by UV Resonant Raman spectroscopy: a step towards the search for biosignatures on Mars

G. Montagnac*[1], J. Hao†[1,2], U. Pedreira-Segade‡[1,3], and I. Daniel§[1]

[1] *Univ Lyon, Ens de Lyon, Univ Lyon 1, CNRS, LGL-TPE, F-69007 Lyon, France*

[2] *now at Department of Marine and Coastal Sciences, Rutgers University, 71 Dudley RD, New Brunswick, NJ08901, USA*

[3] *now at Rensselaer Polytechnic Institute, Troy, NY, USA*

August 26, 2020

Keywords: Deep UV resonant Raman spectroscopy; nucleotides; biosignature; adsorption

Abstract

The payload of Mars 2020 space mission includes a deep UV resonance Raman and fluorescence spectrometer SHERLOC dedicated to the detection of luminescence and Raman signal of condensed carbon and aromatic organics that could potentially be biosignatures. Among minerals detected on Mars surface, phyllosilicates exhibit a strong affinity to organic molecules, including nucleotides, which adsorption mechanisms onto clay minerals have been well documented, whilst there is a lack of an overview of Raman studies of organics adsorbed onto phyllosilicates. Here, we used a deep UV resonant Raman setup to track down the signature of the nucleotide desoxyguanosine-5'-monophosphate (dGMP) adsorbed onto selected minerals, pyrophyllite, chlorite, nontronite and

*Corresponding author: gilles.montagnac@ens-lyon.fr ORCID: https://orcid.org/0000-0001-9938-0282
†ORCID: https://orcid.org/0000-0003-3657-050X
‡ORCID: https://orcid.org/0000-0002-7357-5345
§ORCID: https://orcid.org/0000-0002-1448-7919

montmorillonite. Excitation with a 244 nm laser indeed avoids luminescence of natural phyllosilicates and enhances the Raman signal of the organic molecule chosen here as a model biosignature. However, the deep UV energy of the laser focused onto the samples may induce severe photo-damage to the organic compound without adequate precaution. We used the Raman signature of dGMP to characterize deep UV effect after an irradiation of several minutes (8 - 260 mJ) until a stable spectroscopic signal is detected and could show that it is sensitive to minute amount of dGMP and adsorption mechanism. The effect of widespread oxidants such as perchlorate on the Martian surface is also investigated here because of potential implication in the degradation of nucleotides under UV irradiation. In this study we also discuss the strategy for the detection and preservation of adsorbed biomolecules onto clay surfaces.

1 Introduction

The landing site of the Mars 2020 mission will be the Noachian-aged Jezero crater where high-resolution data from the Mars Reconnaissance Orbiter (MRO) has identified clay-rich fluvial–lacustrine sediments (Ehlmann et al., 2008). This crater contains phyllosilicates including iron-magnesium rich smectite clays (Bibring et al., 2006; Mangold et al., 2007; Poulet et al., 2005). Some regions of interest, particularly rich in clay minerals are planned to be investigated. Like in Earth's soils or any environment resulting from aqueous or hydrothermal alteration of rocks, phyllosilicates are often in close association with organic matter. Multiple studies have shown that in detrital sedimentary systems, preservation of organic compounds through geological time, is favored and enhanced by rapid burial in fine-grained, clay-rich sediments (Farmer and Des Marais, 1999; Meyers and Ishiwatari, 1993).

With this favorable mineralogy and considering Jezero lake as a final closed basin, both primary and transported organics could be sequestered in the clay-rich deposits of the western Jezero delta. These sediments recorded multiple episodes of aqueous activity on early Mars and are likely to preserve organic compounds (Freissinet et al., 2015) and potential biosignatures (Grotzinger et al., 2014). The challenge for the future mission is to enforce the instruments of its payload to track down organic compounds and search for potential biotic signature to secure the science return samples mission.

Deep UV Resonant Raman spectroscopy (DUV-RRS) is a key technique for *in situ* detection and

analyses of organic compounds on Mars. The payload of the Mars 2020 rover includes a proximity science instrument, SHERLOC, dedicated to fluorescence spectroscopy and DUV-RRS (Beegle et al., 2014; Beegle and Bhartia, 2016). The advantage of the latter technique has been demonstrated in the past with short wavelength laser lines (244, 248.6, 266 nm) to characterize aromatic hydrocarbons (Asher and Johnson, 1984), carboxylic acids or amino acids within Mars's regolith simulant (Abbey et al., 2017). With a similar setup, time resolved fluorescence spectroscopy was also applied to discriminate between individual PAHs and kerogen (Eshelman et al., 2018; Shkolyar et al., 2018). Expected detection limits are as low as 10^{-6} and 10^{-3} (organics/minerals in wt/wt) for aromatic and aliphatic organics, respectively; mineral can be identified from their Raman spectra on grains as small as 50 µm (Williford et al., 2018).

Beyond the ability of DUV-RRS to detect organic compounds, it has been recently showed by Sapers et al. (2019) that the technique also has the potential to discriminate the biological compounds in a complex living cell from a mixture of matching aromatic molecules. The DUV-RR biological signature is mostly ascribed to nucleotides and allowed to interrogate the biological *vs.* abiotic origin of the spectra, which are highly variable in meteorites for instance (Steele et al., 2018).

Nested nucleotides onto clay minerals are well documented (Ferris and Hagan Jr., 1986; Ferris et al., 1989; Ferris, 2005). A generalized comprehensive model has recently become available and describes the effect of the phosphate reactivity of nucleotides for their adsorption onto phyllosilicates particles (Pedreira-Segade et al., 2018a), while a suite of high resolution techniques (X-Ray microscopy, surface chemistry, theoretical calculations ...) unveiled the detailed adsorption configuration and location of nucleotides on clay surfaces. Unfortunately, there is still a lack of an overview in Raman studies to investigate the adsorbates.

We therefore used a DUV-RRS setup to characterize the signature of DNA 2'-Deoxyguanosine 5'-Monophosphate (dGMP) as a model nucleotide adsorbed onto selected clay mineral powders. dGMP solutions of different concentrations between 10 mM and 0.4 mM, were mixed with mineral to get aqueous suspensions of 2-4 mg of mineral powder in 1 mL, in order to probe the sensitivity of DUV-RR spectroscopy to known adsorption mechanisms (see details in Feuillie et al. (2013); Pedreira-Segade et al. (2016)). Three groups of phyllosilicates with different crystal structures have been examined in this

study: montmorillonite and nontronite from smectite group, pyrophyllite from talc group and chlorite. All of them have been described in deposits within craters on Mars (Ehlmann et al., 2009; Marzo et al., 2010; Ehlmann and Edwards, 2014). Chlorite and pyrophyllite are common accessory minerals in low-to-medium grade regional metamorphic rocks and their crystallographic structures present major differences with the ones of smectites.

Using deep UV laser at 244 nm wavelength has multiple advantages. First, it staves off the luminescence generated by the minerals and the organics, usually starting around 270 nm and extending to the visible range. Attempts to measure the Raman spectra of such samples with classic visible wavelength (532, 633 nm) have always failed and led to the burning of the sample. Second, deep UV wavelength enhances the Raman signal of some organic molecular structures (Quirico et al., 2008; McMillan et al., 2009; Montagnac et al., 2016). The heterocyclic aromatic ring present in the nucleobase of every nucleotide has a strong $\pi - \pi^*$ transition around 260 nm, which Raman vibration modes are enhanced when excited close to this wavelength. Third, this work also allows to investigate the deleterious effect of high energy deep UV radiations on the preservation of organic biosignatures and get insights into the consequences of the UV radiations received on Mars (Poch et al., 2015; Fornaro et al., 2018a)), as well as the potential implication of perchlorate on the detection and stability of nucleotides under UV irradiation (Fornaro et al., 2018b). Several missions have indeed confirmed the presence of perchlorate at concentrations between 0.5 and 1% in martian soils (e.g., Hecht et al. (2009).

The bactericidal potential of the three combined components that are iron oxides, hydrogen peroxide and UV irradiated perchlorates in Mars's environment has been demonstrated (Wadsworth and Cockell, 2017). However, notable ability to preserve organic molecules has been observed in terrestrial analog sites characterized by halite- and perchlorate-rich hypersaline subsurface deposits, which are widespread on Mars (Fernández-Remolar et al., 2013; Ertem et al., 2017). Perchlorates are highly soluble and are generally preserved in locations characterized by low water activity (Wadsworth and Cockell, 2017). Consequently, we have also conducted adsorption experiment with 4 mM dGMP and additional 0.3 mM $NaClO_4$. All experiments were performed at natural pH close to 7, in agreement with the circumneutral pH conditions proposed in many locations on Mars, such as the Gale crater (Grotzinger et al., 2014). More acidic conditions have also been proposed, like in the Burns formation, Meridiani Planum

(McLennan et al., 2005) but were not investigated in the current contribution.

This work points out to the ability and limits of DUV-RRS as an *in situ* technique to detect organic signatures and potential specific biosignatures in the search of traces of life for future missions to Mars. Protocols still need to be improved and applied carefully to avoid damaging organic molecules, which would definitely preclude any assessment of their potential biological origin.

2 Sample selection and methods

Adsorption of nucleotides onto clay minerals

The nucleotide 2'-Deoxyguanosine 5'-Monophosphate (dGMP) is composed of a phosphate group, a sugar moiety and a guanine nucleobase. Nucleotides exhibits different chemical compositions depending on nucleobase and presence or absence of hydroxyl group on the sugar moiety in RNA and DNA, respectively. Nevertheless, previous detailed studies have shown that they behave as homologous molecules with respect to their adsorption mechanism on clay minerals under circumneutral pH (see review by Pedreira-Segade et al. (2018a) and references therein). Under the conditions investigated in the present study, dGMP is tightly adsorbed through ligand exchange between the phosphate group and the hydroxyls of the broken edges of phyllosilicates. It is strong enough to prevent desorption upon dilution. This similarity in adsorption mechanism allowed us to perform all experiments on dGMP and consider the results as representative of those for nucleotides in general.

The dGMP sodium salt was purchased from Sigma Aldrich™ with high purity (>99%) and dissolved into deionized water to reach the targeted concentrations, i.e., 10, 4, 2 and 0.4 mM dGMP. Montmorillonite (SAz1, from Arizona, USA, $(Si_{7.95}Al_{0.05})(Al_{2.75}Fe^{3+}_{0.17}Mg_{1.07})O_{20}(OH)_4Na_{1.11}$; see Paineau et al. (2011)), nontronite (NAu2, from Australia, $(Si_{7.55}Al_{0.16}Fe^{3+}_{0.29}(Al_{0.34}Fe^{2+}_{3.54}Mg_{0.05})O_{20}(OH)_4Na_{0.72}$; see Gates et al. (2002)), chlorite (CCa-2 ripidolite, from California, USA, $(Si_{2.65}Al_{1.35})(Mg_{2.92}Al_{1.15}Fe^{3+}_{0.21}Fe^{2+}_{1.68}Mn_{0.01})O_{10}(OH)_8$, see Gailhanou et al. (2009)) used in the present work were purchased from the Source Clay Minerals Repository of the Clay Mineral Society (Purdue University, USA). Pyrophyllite was prepared from Stumat™ samples. The smectite group is represented by montmorillonite and nontronite minerals. They have a common stacking se-

quence T-Oc-T-INT (T, tetrahedral layer, Oc, octahedral layer and INT, inter-layer), in which INT sites are filled by cations such as Na^+,K^+,Ca^{2+},Li^+ and/or $Mg(H_2O)_6$ units and sandwiched between T-Oc-T layers. Pyrophyllite ($Al_2Si_4O_{10}(OH)_2$), from the talc group has a T-Oc-T staking sequence and the chlorite group has a general structure with layers of edge-sharing $(Mg,Fe,Al)(OH)_6$ octahedra sandwithed in between T-Oc-T layers. All minerals have been purified and characterized in details for their surface physical and chemical properties, e.g. purity, specific surface area, cation exchange capacity, etc. in earlier studies (Table S2) (Feuillie et al., 2013; Pedreira-Segade et al., 2016). The sub-micron size clay particles were stored as homogeneous mineral suspensions in deionized water, with controlled mineral concentration before use in adsorption experiment.

Adsorption of dGMP onto phyllosilicates was performed through batch experiments under ambient conditions of pressure and temperature, at natural pH close to 7. The pH was close to neutrality but the solutions are not buffered. The dGMP solution was mixed with carefully weighted minerals (2-4 mg ±10 µg) in 2 mL Eppendorf safe-lock tubes. The tubes were vortexed for 10 s to achieve homogenization and then allowed to stand in a dark water bath at 25 °C for 24 h to ensure adsorptionequilibrium. Afterwards, the suspensions were centrifuged for 25 min at 16,100 g (acceleration of gravity). Finally, the separated supernatant was analyzed using UV spectrophotometry at 260 nm to check that the equilibrium concentration of dGMP was consistent with our previous detailed studies (Feuillie et al., 2013; Pedreira-Segade et al., 2016). The pellet of adsorbed dGMP onto the clay fine grains was re-suspended in pure water, deposited onto a silica glass slide and was allowed to air dry prior to Raman measurement. As above mentioned, the strong binding of the nucleotides on the clay platelets precluded desorption. This procedure led to the deposition of a thin film homogeneous and flat enough to be suitable for Raman measurements with our UV setup.

DUV-RRS and UV irradiation damage

A LabRam HR800 UV from Horiba™ manufacturer was used for all UV measurements. The Raman diffusion was excited with an argon ion laser tuned blue (488 nm) and frequency doubled at 244 nm by a BBO crystal in an external cavity (Spectra Physics™ Wavetrain). The laser beam was focused onto the sample with an OFR™ LMU x40 objective. The probe spot has a diameter of around 3 μm. We used a

3600 grooves/mm grating to collect Raman spectra in the wavelength ranging from 800 to 1900 cm^{-1}. We selected this spectral range as the Raman fingerprint of nucleotide signature. Moreover symmetric stretching vibrations of phosphate and chlorate are expected to lie in between 900 and 1200 cm^{-1}. The second order of the spectrum is characterized by a very low signal in the range of 2500 to 3500 cm^{-1} with Raman bands at 2800, 2955, 3070 cm^{-1} superimposed on a broad signal spreading over the whole spectral range. The dielectric Raman filter has a cutoff around 400 cm^{-1} and prevents measurements below. With this setup, the spectral resolution was as high as 1 cm^{-1}.

We present here DUV-RR spectra with limited pre-processing treatments. A linear baseline was subtracted to the raw data over the whole wavenumber range. In the deep UV range, the Raman signal usually has no background. All spectra have been normalized to maximum peak intensity. In most spectra in this study, the most intense peak was at 1490 cm^{-1} except a few samples, where the 1600 cm^{-1} band was very intense (pyrophyllite and sample of 0.4 mM of dGMP onto montmorillonite).

During Raman measurements and despite all efforts, the absorption of ultraviolet (UV) light by nucleotides caused inevitable damage to the molecule (Kumamoto et al., 2011). The static exposure to deep UV light induces instantaneous degradation of the molecule and creates a characteristic Raman signature of aromatic clusters composed of a strong, broad and asymmetric band with a maximum centered around 1600 cm^{-1}. In order to minimize this deleterious effect and investigate the degradation of the organic molecule by UV, we used a spinning stage to hold sample films and keep the laser focused on (Wang et al., 2011). The sample film is rotating under the standing still objective and the rotation speed was adjusted to 20 rpm. Thus, the surface probed by the laser beam during the acquisition time is a circle with radius given by the offset distance between the axis of the objective and the rotating stage one (2.5 mm). The laser spot on the sample has a waist diameter around 3 μm. Therefore, the surface of the sample irradiated and probed during Raman acquisition is around 4.7×10^{-4} cm^2. The signal is the average of the Raman diffusion on this surface that is much larger than the laser spot size (7 μm^2). This also minimizes the potential effects of sample inhomogeneity. According to Carrier et al. (2019), the depth penetration of deep UV laser beam (around 250 nm, UVC) could be 500 µm or higher in minerals like kaolinite or gypsum. However, changing the focus of the laser across the film surface systematically induced an exponential decrease of the Raman signal. Thus, all measurements were performed at the

focusing point of the laser on the surface of the samples. DUV-RR spectra were acquired after (1) 20 seconds of acquisition time, (2) 200 seconds of acquisition time. To follow the evolution of the signal as a function of exposure time, we monitored and plotted Raman spectra as 2D images with time lapse of 10 seconds acquisitions during 400 seconds.

Working with a mean power of 0.4 to 1.3 mW (0.8×10^3 to 2.7×10^3 mW/cm^2) during 20 seconds up to 200 seconds, the maximum amount of energy deposited on the samples is 5.5×10^5 mJ/cm^2. This value is 3 magnitudes greater than the energy of the natural UV flux on the surface of Mars as estimated by Patel et al. (2003, 2002). Assuming a dust free atmosphere at the noontime equator, the light flux is of 1.4×10^{15} photons s^{-1} cm^{-2}, corresponding to 2.2×10^2 mJ/cm^2 for 200 seconds of exposition.

3 Results

The film of pure dGMP dried from a 10 mM solution, displays intense DUV-RR modes. These modes are associated to the in-plane vibrations of the purine heterocycles. We compare these spectra with the non-resonant one acquired at 532 nm, on a dGMP solution close to saturation (Figure 1). The DUV-RR spectrum has enhanced Raman bands with similar positions as the non-resonant Raman spectrum. These modes are visible even at low concentration when dGMP is adsorbed onto clay minerals (Figure 2), whilst they are utterly invisible with 532 nm excitation because of a huge luminescence background and strong absorption of visible light, burning the film.

The strongest Raman modes are listed (ν_1 to ν_6 in Figure 1 and Table 1) and attributed based on previous assignment (Fodor et al., 1985; Russell et al., 1995; Lee et al., 2017). Stripes with the same color pallet are used throughout this study to highlight these different wavenumber ranges. The 1490 cm^{-1} peak (ν_4) is primarily related to three stretching modes of C2=N3 + C4=C5 + N7=C8 of the nucleobase. This mode extends across both rings in guanine. Another vibration mode at ca. 1360 cm^{-1} (ν_3) also involves both the pyrimidine and imidazole rings, C2=N3 C4-N9. The 1325 cm^{-1} peak (ν_2) corresponds to a pure imidazole ring stretching mode and is localized around the N7 nitrogen atom. Other strong modes at 1570 (ν_5) and 1605 cm^{-1} (ν_6) are pure pyrimidine ring modes. The last one also involves the NH_2 group scissoring with the C2 carbon atom of the pyrimidine cycle. Eventually, we have highlighted in gold color the possible region (ν_1) attributed to the degenerated mode of PO_4 stretching

in dGMP molecule (Ghomi and Taillandier, 1985). The weak band at 1700 cm^{-1} is attributed to C6=O vibration (Fodor et al., 1985).

The spectra in the bottom right part of Figure 1 illustrate the photochemical impact of UV-irradiation on dGMP nucleotide, that has two major effects:

1. A small swelling of the background between 1200 and 1700 cm^{-1}. This background is related to an asymmetric broad band with a maximum around 1600 cm^{-1} that is typical of sp2 bonds in aromatic clusters (Ferrari and Robertson, 2001) and reveals a possible damage of some dGMP molecules. This band grows and stabilizes after 100 seconds exposure but doesn't overlap with the 1605 and 1570 cm^{-1} peaks of pyrimidine. Working with higher laser power of 1.3 mW induces a similar but more intense swelling of the baseline. Under these conditions, positions and FWHM of the resonant modes are affected after only a few seconds of exposure, and well visible with 20 seconds of acquisition only (26 mJ). During an acquisition of 600 seconds or longer with low power ca. 0.4 mW (240 mJ of energy), there is no evidence of damage except this slight swelling of the background.

2. The UV irradiation induces a softening of the backbone of the dGMP molecule, described as a "floppy" effect by Lee et al. (2017). As a consequence, the two Raman modes extending across both rings (ν_3 and ν_4) are decreasing in intensity, whereas ν_2 and ν_6 increase and particularly the last one, NH_2 scissoring.

There is a power threshold beyond which the vibrational signature is definitely altered. We choose to work under the harshest conditions, though without burning the organic molecule. Spectra do not evolve anymore for acquisition times of 200 seconds (260 mJ) and longer. In the range between 950-1150 cm^{-1}, broad bands appear, assumed to be representatives of the degenerated stretching modes of phosphate unbounded to mineral cations. A supplementary non-attributed band appears in dGMP spectrum around 1505 cm^{-1} with 1.3 mW of laser during 200 seconds. We also observe this band on dGMP adsorbed onto smectite samples (see Figures 2, 3 and 5).

Effect of host mineral

Figure 2 displays DUV-RR spectra of dried dGMP (10 mM) adsorbed onto phyllosilicates, i.e., montmorillonite, nontronite (smectite group), pyrophyllite (talc group) and chlorite. The spectra of dGMP adsorbed onto swelling clay minerals have the highest signal to noise ratio. Next is on the chlorite substratum and eventually on the pyrophyllite. DUV-RR spectra of nontronite and montmorillonite are similar considering wavenumber positions and FWHM of Raman bands. A new non-attributed band is observed at ca. 1505 cm^{-1} with these samples. The strong mode at 1600 cm^{-1} in the pyrophyllite is attributed to possible contamination of the mineral surface before adsorption of dGMP. This peak is a typical signature of the G band of carbonaceous matter. It is also visible in the non-resonant spectra of this mineral.

The quality of the DUV-RR spectra is very encouraging and directly reflects adsorption mechanisms. Clay particles in the initial suspension potentially offer basal, inter-layer or lateral surfaces to adsorb the organic molecules of dGMP with different surface sites or processes, while nucleotides exhibit mainly phosphate and nucleobase reactive groups sensitive to pH or hydrogen bonding conditions.

In our experiments at ambient conditions of pressure, temperature, and natural pH, all nucleotides adsorb on the lateral surfaces of the clay minerals through ligand exchange between their phosphate group and the hydroxyl groups of the broken bonds of the minerals' edges until their reactive sites are fully covered. This corresponds to an equilibrium concentration of nucleotides of ca. 1 mM dGMP and adsorption densities between 1.3 and 2.5 µmol/m^2 (see Figure 1 in Pedreira-Segade et al. (2016)). This is the maximum adsorption of dGMP on non-swelling phyllosilicates such as pyrophyllite and chlorite, which display here the lowest DUV-RR intensity even with an initial nucleotide concentration as high as 10 mM.

However, for the swelling clay minerals (smectites) montmorillonite-SAz1 and nontronite-NAu2, the DUV-RR intensity is stronger and consistent with the increased adsorbed densities measured at equilibrium concentrations in excess of 1 mM. Beyond 1 mM, their adsorption density becomes linear as a function of the equilibrium concentration, indicating the opening of a second low-energy adsorption regime that has not yet been characterized and potentially involves multiple layers of nucleotides on the lateral surfaces or adsorption on the large basal surfaces of the swelling clay minerals. Characterization

of the latter mechanisms is beyond the scope of the present contribution. The possible adsorption of the nucleotide on the basal planes of swelling clay minerals has been assessed through classical molecular dynamics (MD) simulations by Mignon et al. (2019) in this same special issue. In this configuration, the nucleotide molecule also binds with the cations of the basal surfaces of the minerals and some vibrations of the molecule are reinforced, giving strongest Raman bands on montmorillonite and nontronite samples.

Effect of nucleotide concentration

The DUV-RR spectra of the dry films of dGMP adsorbed onto montmorillonite are plotted in Figure 3, for three initial concentrations of 10, 2 and 0.4 mM. The quality of the spectra is very good and the signal of dGMP clearly identified even at the lowest concentration of 0.4 mM. The 1490 cm^{-1} peak is still visible and well resolved despite a decrease in intensity by a factor 2. At the lowest initial concentration, all other modes tend to broaden and noise increases. Unfortunately, there is no evidence of a simple relation between the initial concentration of dGMP in the solution and the density of nucleotide adsorbed onto the montmorillonite surfaces.

One may notice that a strong signal appears in the range of PO_4 vibration, 900-1200 cm^{-1} (Ghomi and Taillandier, 1985), for the lowest dGMP initial concentration. This certainly reflects the different adsorption mechanisms of dGMP onto montmorillonite at low and high concentrations. At low equilibrium concentration below 1 mM, under the current experimental conditions, nucleotides and thereby dGMP adsorb only on the high energy sites of the lateral surface of the phyllosilicates, whether swelling or not. As mentioned above, the adsorption occurs through ligand exchanges between the phosphate of the nucleotide and the dangling bonds of the edges of the minerals. This ligand exchange is likely to enhance the Raman signal of the phosphate, due to the lack of direct interaction between the aromatic cycles and the phyllosilicates' basal surface.

However, at higher equilibrium concentrations in excess of 1 mM other adsorption mechanisms take place. They still require detailed investigation but these processes are likely to involve the adsorption of nucleotides on the basal surface of swelling clay minerals only, depending on the composition of the layers that screen the negatively charged surface in contact with the solutes (Mignon et al., 2019; Pedreira-Segade et al., 2018b). Despite the lack of details, it precludes the adsorption of the negatively charged

phosphate group and likely involves the rather neutral guanine nucleobase as illustrated in Figure 3 by the strong stretching vibrations of the nucleobase for 10 and 2 mM initial concentration.

Effect of mineral grain size

Powder of pyrophyllite (10 µm size) was used to prepare a batch of dry films samples. In parallel, we crushed this powder to obtain smaller grain size (ca. 1 µm) of this mineral and prepared the dry films. Spectra collected onto crushed micron size pyrophyllite have less intensity compared to the ones of the original powder with coarser grains despite a larger reactive surface (Figure 4). It is a direct consequence of the diffusion of light lost in fine grains. However for long acquisitions of 200 seconds, the signal of dGMP is better preserved on the fine powder sample. The 1325, 1360, 1490 and 1570 cm^{-1} bands are stronger while the one at 1600 cm^{-1} overwrites the signal in the original coarse powder sample. This effect could be explained by the increased available surface of mineral to adsorb and protect dGMP. In this study we only investigated the effect of grain size with non-swelling mineral sample.

Effect of perchlorate

Dry films were obtained from montmorillonite powder with a solution of 4 mM of dGMP nucleotides and additional 0.3 mM of $NaClO_4$ to investigate the influence of perchlorate on the stability of nucleotide. Perchlorate has a very intense peak at 930 cm^{-1} and two weak peaks at 1095 and 1148 cm^{-1} and no signal that overlaps the fingerprint of dGMP. In Figure 5 we compare the DUV-RR spectra obtained after 400 seconds of laser exposition and higher mean power (1.3 mW).

The dGMP signature is well preserved all along the acquisition time, in presence of perchlorate. Raman bands are narrow, the background between 1200 and 1800 cm^{-1} is low, the 1505 cm^{-1} peak still appears as a shoulder of the strong 1490 cm^{-1} peak. Two effects could have an influence on the preservation of the dGMP signal (1) the effect of salinity on the adsorption of nucleotides onto phyllosilicates (Pedreira-Segade et al., 2018b) (2) the hydrogen bonding between dGMP molecule and perchlorate. It has been demonstrated by Toyama et al. (2005), that the UV-RR intensity of 2',3',5'-tri-O-acetyladenisine (adenine AcAdo) is correlated to hydrogen bonding at the proton acceptor N1, N3 and N7 and donor C6-NH_2. We probably observe a similar effect in the present experiment with dGMP,

i.e., the strength of hydrogen bonding between dGMP and perchlorate is reinforced and stabilizes the UV-RR bands of the organic molecule. In presence of perchlorate, the floppy effect due to UV irradiation is still visible on the Raman signal (ν_3 and ν_4 are decreasing, ν_6 is increasing) but much weaker and there is no clear evidence of degradation of the molecule.

Evolution of the DUV-RR signal is monitored with reconstructed 2D images and surface images from acquisition sequences of 10 seconds time lapse. Figure 6 shows a comparison of the evolution of dGMP onto montmorillonite surface with and without perchlorate. There is no evidence of broadening of the Raman bands with time exposition in 2D image in the presence $NaClO_4$ perchlorate (Figure 6B and D). Intensities decrease but less than without perchlorate and stabilize quickly after 100 seconds (Figure 6A and C). The "crenelated" appearance of the surface image is attributed to the slight roughness of the dry film of samples prepared with perchlorate (Figure 6C). The film obtained with $NaClO_4$ was pleated and during rotation of the stage, the focus was occasionally slightly out and the signal became weaker, leading this grooved shape to the surface image.

4 Conclusion and perspective for Mars instruments

We demonstrate in this preliminary work, that DUV-RRS offers a powerful way to track down nucleotide (dGMP), an essential "building block" of life adsorbed onto clay minerals substratum. The ability of phyllosilicates for nucleotides adsorption has been well documented for decades but no convincing Raman measurements had yet been performed. We have here examined the capacity and limits of this technique for specific detection of nucleotides as a potential biosignature.

To evaluate the effect of massive UV laser irradiation inherent to the technique, we investigated the evolution of the Raman signal produced by the dGMP adsorbed onto clay minerals. The DUV-RR signal of samples positioned on a spinning stage, was monitored until a stable signal was obtained. Very good resonant spectra of nucleotides were indeed obtained down to low initial concentration of 0.4 mM.

The DUV-RR peak intensities of nucleotide molecule may furthermore serve as a sensitive probe of the interactions with the clay minerals. At normal temperature and pressure conditions and pH$\approx$7, dGMP adsorbed onto swelling clay minerals studied here (montmorillonite, nontronite), has a stronger Raman signal than when adsorbed on pyrophillite or cholorite. Our DUV-RR measurements also confirm

the low energy adsorption process of dGMP likely onto the basal surfaces of swelling clay minerals for equilibrium concentration in excess of 1 mM. The dGMP molecule binds to the basal surfaces of the swelling clay mineral in addition to the lateral surfaces. At 0.4 mM (under 1 mM) of initial dGMP concentration, Raman bands of the phosphate group are well detected, reflecting mostly the adsorption mechanism of dGMP by ligand exchange between the phosphate group and the dangling bonds of the lateral surfaces of the montmorillonite clay.

In the Martian context and next mission Mars 2020, our setup can't obviously be considered as a duplicate of the SHERLOC instrument but the present measurements share some of SHERLOC's challenges and will inform SHERLOC's field measurements. We have demonstrated the benefits of the DUV-RR technique to deliver a fluorescence-free signal in the Raman range and an intense resonance or pre-resonance Raman signal of some potentially biotic molecules like nucleotides adsorbed onto clay minerals. The present results show that it is possible to not only detect nucleotides *in situ* (onto the clay films), but also to distinguish between different adsorption mechanisms. The major differences between our setup and a fieldable planetary instrument are the spectral resolution and the fluence of the laser source device. Our successful protocol relies chiefly on a permanent movement of the sample under the laser beam during analysis that virtually increases the fluence of the laser source and successfully avoided thermal decomposition of the sample. We have worked here with a maximum of 550×10^2 J/cm^2 to be compared with 59 J/cm^2 for a SHERLOC-type instrument (Abbey et al., 2017). This suggests that the capacity for field measurements and potential of characterization of adsorbed nucleotides by DUV-RR spectroscopy on Mars could potentially benefit from strategic adjustment to minimize the energy deposited by the laser on the sample at one location and improve the preservation of the pristine biosignature of organics adsorbed on clay minerals. Since perchlorate is widely spread in martian soils and may also alter the preservation of biomolecules, we measured the effect of perchlorate on the stability of nucleotide adsorbed onto swelling clay minerals and could show that the addition of perchlorate was actually beneficial, due to enhanced hydrogen bonding between perchlorate and the purine heterocycle of dGMP.

Acknowledgments

The Raman facility in Lyon (France) is supported by the Institut National des Sciences de l'Univers (INSU). This work is also financially supported by The French National Research Agency through the PREBIOM (Primitive Earth - Biomolecules Interacting with Hydrothermal Oceanic Minerals) project ANR-15-CE31-0010. J. H. acknowledges the postdoctoral fellowship from LABEX Lyon Institute of Origins (ANR-10-LABX-0066) of the Université de Lyon within the program "Investissements d'Avenir" (ANR-11-IDEX-0007) of the French government operated by the National Research Agency (ANR).

References

Abbey, W. J., Bhartia, R., Beegle, L. W., DeFlores, L., Paez, V., Sijapati, K., Sijapati, S., Williford, K., Tuite, M., Hug, W., and Reid, R. Deep UV Raman spectroscopy for planetary exploration: The search for in situ organics. *Icarus*, 290:201 – 214, 2017. ISSN 0019-1035. doi: https://doi.org/10.1016/j.icarus.2017.01.039. URL http://www.sciencedirect.com/science/article/pii/S0019103516306169.

Asher, S. and Johnson, C. Raman spectroscopy of a coal liquid shows that fluorescence interference is minimized with ultraviolet excitation. *Science*, 225(4659):311, 1984.

Beegle, L. W., Bhartia, R., DeFlores, L. P., Asher, S. A., Burton, A. S., Clegg, S. M., Conrad, P. G., Edgett, K. S., Ehlmann, B. L., Langenhorst, F., Fries, M., Nealson, K. H., Popp, J., Sobron, P., Steele, A., Wiens, R. C., and Williford, K. H. SHERLOC: Scanning habitable environments with Raman & luminescence for organics & chemicals, an investigation for 2020. In *AGU Fall Meeting Abstracts*, volume 2014, pages P24A–06, 2014.

Beegle, L. and Bhartia, R. SHERLOC: An investigation for Mars 2020. In *EGU General Assembly Conference Abstracts*, EGU General Assembly Conference Abstracts, pages EPSC2016–11215, 2016.

Bibring, J.-P., Langevin, Y., Mustard, J. F., Poulet, F., Arvidson, R., Gendrin, A., Gondet, B., Mangold, N., Pinet, P., Forget, F., Berthé, M., Bibring, J.-P., Gendrin, A., Gomez, C., Gondet, B., Jouglet, D., Poulet, F., Soufflot, A., Vincendon, M., Combes, M., Drossart, P., Encrenaz, T., Fouchet, T., Merchiorri, R., Belluci, G., Altieri, F., Formisano, V., Capaccioni, F., Cerroni, P., Coradini, A., Fonti, S., Korablev, O., Kottsov, V., Ignatiev, N., Moroz, V., Titov, D., Zasova, L., Loiseau, D., Mangold, N., Pinet, P., Douté, S., Schmitt, B., Sotin, C., Hauber, E., Hoffmann, H., Jaumann, R., Keller, U., Arvidson, R., Mustard, J. F., Duxbury, T., Forget, F., and Neukum, G. Global mineralogical and aqueous Mars history derived from OMEGA/Mars Express data. *Science*, 312(5772):400–404, 2006. ISSN 0036-8075. doi: 10.1126/science.1122659. URL https://science.sciencemag.org/content/312/5772/400.

Carrier, B. L., Abbey, W. J., Beegle, L. W., Bhartia, R., and Liu, Y. Attenuation of ultraviolet radiation in rocks and minerals: implications for Mars science. *Journal of Geophysical Research: Planets*, 124(10):2599–2612, 2019. doi: 10.1029/2018JE005758. URL https://agupubs.onlinelibrary.wiley.com/doi/abs/10.1029/2018JE005758.

Ehlmann, B. L. and Edwards, C. S. Mineralogy of the martian surface. *Annual Review of Earth and Planetary Sciences*, 42(1):291–315, 2014. doi: 10.1146/annurev-earth-060313-055024. URL https://doi.org/10.1146/annurev-earth-060313-055024.

Ehlmann, B. L., Mustard, J. F., Fassett, C. I., Schon, S. C., Head III, J. W., Des Marais, D. J., Grant, J. A., and Murchie, S. L. Clay minerals in delta deposits and organic preservation potential on Mars. *Nature Geoscience*, 1(6):355–358, 2008. ISSN 1752-0908. URL https://doi.org/10.1038/ngeo207.

Ehlmann, B. L., Mustard, J. F., Swayze, G. A., Clark, R. N., Bishop, J. L., Poulet, F., Des Marais, D. J., Roach, L. H., Milliken, R. E., Wray, J. J., Barnouin-Jha, O., and Murchie, S. L. Identification of hydrated silicate minerals on mars using mro-crism: Geologic context near nili fossae and implications for aqueous alteration. *Journal of Geophysical Research: Planets*, 114(E2), 2009. doi: 10.1029/2009JE003339. URL https://agupubs.onlinelibrary.wiley.com/doi/abs/10.1029/2009JE003339.

Ertem, G., Ertem, M. C., McKay, C. P., and Hazen, R. M. Shielding biomolecules from effects of radiation by Mars analogue minerals and soils. *International Journal of Astrobiology*, 16(3):280–285, 2017. doi: 10.1017/S1473550416000331.

Eshelman, E., Daly, M., Slater, G., and Cloutis, E. Detecting aromatic compounds on planetary surfaces using ultraviolet time-resolved fluorescence spectroscopy. *Planetary and Space Science*, 151:1 – 10, 2018. ISSN 0032-0633. doi: https://doi.org/10.1016/j.pss.2017.09.003. URL http://www.sciencedirect.com/science/article/pii/S0032063317300983.

Farmer, J. D. and Des Marais, D. J. Exploring for a record of ancient Martian life. *Journal of Geophysical Research: Planets*, 104(E11):26977–26995, 1999. doi: 10.1029/1998JE000540. URL https://agupubs.onlinelibrary.wiley.com/doi/abs/10.1029/1998JE000540.

Fernández-Remolar, D. C., Chong-Díaz, G., Ruíz-Bermejo, M., Harir, M., Schmitt-Kopplin, P., Tziotis, D., Gómez-Ortíz, D., García-Villadangos, M., Martín-Redondo, M. P., Gómez, F., Rodríguez-Manfredi, J. A., Moreno-Paz, M., De Diego-Castilla, G., Echeverría, A., Urtuvia, V. N., Blanco, Y., Rivas, L., Izawa, M. R. M., Banerjee, N. R., Demergasso, C., and Parro, V. Molecular preservation in halite- and perchlorate-rich hypersaline subsurface deposits in the Salar Grande basin (Atacama Desert, Chile): Implications for the search for molecular biomarkers on Mars. *J. Geophys. Res. Biogeosci.*, 118(2):922–939, 2013. ISSN 2169-8953. doi: 10.1002/jgrg.20059. URL https://doi.org/10.1002/jgrg.20059.

Ferrari, A. C. and Robertson, J. Resonant Raman spectroscopy of disordered, amorphous, and diamondlike carbon. *Phys. Rev. B*, 64:075414, 2001. doi: 10.1103/PhysRevB.64.075414. URL https://link.aps.org/doi/10.1103/PhysRevB.64.075414.

Ferris, J. P. Mineral catalysis and prebiotic synthesis: montmorillonite-catalyzed formation of RNA. *Elements*, 1(3):145–149, 2005. ISSN 1811-5209. doi: 10.2113/gselements.1.3.145. URL https://doi.org/10.2113/gselements.1.3.145.

Ferris, J. and Hagan Jr., W. The adsorption and reaction of adenine nucleotides on montmorillonite. *Origins of Life and Evolution of the Biosphere*, 17(1):69–84, 1986. doi: 10.1007/BF01809814. cited By 49.

Ferris, J., Ertem, G., and Agarwal, V. The adsorption of nucleotides and polynucleotides on montmorillonite clay. *Origins of Life and Evolution of the Biosphere*, 19(2):153–164, 1989. doi: 10.1007/BF01808149. cited By 71.

Feuillie, C., Daniel, I., Michot, L. J., and Pedreira-Segade, U. Adsorption of nucleotides onto Fe–Mg–Al rich swelling clays. *Geochimica et Cosmochimica Acta*, 120: 97 – 108, 2013. ISSN 0016-7037. doi: https://doi.org/10.1016/j.gca.2013.06.021. URL http://www.sciencedirect.com/science/article/pii/S0016703713003554.

Fodor, S. P. A., Rava, R. P., Hays, T. R., and Spiro, T. G. Ultraviolet resonance Raman spectroscopy of the nucleotides with 266-, 240-, 218-, and 200-nm pulsed laser excitation. *J. Am. Chem. Soc.*, 107(6):1520–1529, 1985. ISSN 0002-7863. doi: 10.1021/ja00292a012. URL https://doi.org/10.1021/ja00292a012.

Fornaro, T., Boosman, A., Brucato, J. R., ten Kate, I. L., Siljeström, S., Poggiali, G., Steele, A., and Hazen, R. M. UV irradiation of biomarkers adsorbed on minerals under Martian-like conditions: Hints for life detection on Mars. *Icarus*, 313:38 – 60, 2018a. ISSN 0019-1035. doi: https://doi.org/10.1016/j.icarus.2018.05.001. URL http://www.sciencedirect.com/science/article/pii/S0019103517307789.

Fornaro, T., Steele, A., and Brucato, J. R. Catalytic/protective properties of martian minerals and implications for possible origin of life on Mars. *Life*, 8(4), 2018b. ISSN 2075-1729. doi: 10.3390/life8040056. URL https://www.mdpi.com/2075-1729/8/4/56.

Freissinet, C., Glavin, D. P., Mahaffy, P. R., Miller, K. E., Eigenbrode, J. L., Summons, R. E., Brunner, A. E., Buch, A., Szopa, C., Archer Jr., P. D., Franz, H. B., Atreya, S. K., Brinckerhoff, W. B., Cabane, M., Coll, P.,

Conrad, P. G., Des Marais, D. J., Dworkin, J. P., Fairén, A. G., François, P., Grotzinger, J. P., Kashyap, S., ten Kate, I. L., Leshin, L. A., Malespin, C. A., Martin, M. G., Martin-Torres, F. J., McAdam, A. C., Ming, D. W., Navarro-González, R., Pavlov, A. A., Prats, B. D., Squyres, S. W., Steele, A., Stern, J. C., Sumner, D. Y., Sutter, B., Zorzano, M.-P., and the MSL Science Team. Organic molecules in the Sheepbed Mudstone, Gale Crater, Mars. *Journal of Geophysical Research: Planets*, 120(3):495–514, 2015. doi: 10.1002/2014JE004737. URL https://agupubs.onlinelibrary.wiley.com/doi/abs/10.1002/2014JE004737.

Gailhanou, H., Rogez, J., van Miltenburg, J. C., van Genderen, A. C. G., Grenèche, J. M., Gilles, C., Jalabert, D., Michau, N., Gaucher, E. C., and Blanc, P. Thermodynamic properties of chlorite cca-2. heat capacities, heat contents and entropies. *Geochimica et Cosmochimica Acta*, 73(16):4738–4749, 2009. doi: https://doi.org/10.1016/j.gca.2009.04.040. URL http://www.sciencedirect.com/science/article/pii/S0016703709003512.

Gates, W. P., Slade, P. G., Manceau, A., and Lanson, B. Site occupancies by iron in nontronites. *Clays and Clay Minerals*, 50(2):223–239, 2002. URL https://doi.org/10.1346/000986002760832829.

Ghomi, M. and Taillandier, E. Normal coordinate analysis of 5'-dGMP and its deuterated derivatives. *European Biophysics Journal*, 12(3):153–162, 1985. ISSN 1432-1017. doi: 10.1007/BF00254073. URL https://doi.org/10.1007/BF00254073.

Grotzinger, J. P., Sumner, D. Y., Kah, L. C., Stack, K., Gupta, S., Edgar, L., Rubin, D., Lewis, K., Schieber, J., Mangold, N., Milliken, R., Conrad, P. G., DesMarais, D., Farmer, J., Siebach, K., Calef, F., Hurowitz, J., McLennan, S. M., Ming, D., Vaniman, D., Crisp, J., Vasavada, A., Edgett, K. S., Malin, M., Blake, D., Gellert, R., Mahaffy, P., Wiens, R. C., Maurice, S., Grant, J. A., Wilson, S., Anderson, R. C., Beegle, L., Arvidson, R., Hallet, B., Sletten, R. S., Rice, M., Bell, J., Griffes, J., Ehlmann, B., Anderson, R. B., Bristow, T. F., Dietrich, W. E., Dromart, G., Eigenbrode, J., Fraeman, A., Hardgrove, C., Herkenhoff, K., Jandura, L., Kocurek, G., Lee, S., Leshin, L. A., Leveille, R., Limonadi, D., Maki, J., McCloskey, S., Meyer, M., Minitti, M., Newsom, H., Oehler, D., Okon, A., Palucis, M., Parker, T., Rowland, S., Schmidt, M., Squyres, S., Steele, A., Stolper, E., Summons, R., Treiman, A., Williams, R., Yingst, A., and Team, M. S. A habitable fluvio-lacustrine environment at Yellowknife Bay, Gale Crater, Mars. *Science*, 343(6169), 2014. ISSN 0036-8075. doi: 10.1126/science.1242777. URL https://science.sciencemag.org/content/343/6169/1242777.

Hecht, M. H., Kounaves, S. P., Quinn, R. C., West, S. J., Young, S. M. M., Ming, D. W., Catling,

D. C., Clark, B. C., Boynton, W. V., Hoffman, J., DeFlores, L. P., Gospodinova, K., Kapit, J., and Smith, P. H. Detection of perchlorate and the soluble chemistry of Martian soil at the Phoenix lander site. *Science*, 325(5936):64–67, 2009. ISSN 0036-8075. doi: 10.1126/science.1172466. URL https://science.sciencemag.org/content/325/5936/64.

Kumamoto, Y., Taguchi, A., Smith, N. I., and Kawata, S. Deep UV resonant Raman spectroscopy for photodamage characterization in cells. *Biomedical optics express*, 2(21483614):927–936, 2011. ISSN 2156-7085. URL https://www.ncbi.nlm.nih.gov/pmc/articles/PMC3072131/.

Lee, J., Challa, J. R., and McCamant, D. W. Ultraviolet light makes dGMP floppy: Femtosecond stimulated Raman spectroscopy of 2'-deoxyguanosine 5'-monophosphate. *J. Phys. Chem. B*, 121(18):4722–4732, 2017. ISSN 1520-6106. doi: 10.1021/acs.jpcb.7b01694. URL https://doi.org/10.1021/acs.jpcb.7b01694.

Mangold, N., Poulet, F., Mustard, J. F., Bibring, J.-P., Gondet, B., Langevin, Y., Ansan, V., Masson, P., Fassett, C., Head III, J. W., Hoffmann, H., and Neukum, G. Mineralogy of the Nili Fossae region with OMEGA/Mars Express data: 2. Aqueous alteration of the crust. *Journal of Geophysical Research: Planets*, 112(E8), 2007. doi: 10.1029/2006JE002835. URL https://agupubs.onlinelibrary.wiley.com/doi/abs/10.1029/2006JE002835.

Marzo, G. A., Davila, A. F., Tornabene, L. L., Dohm, J. M., Fairén, A. G., Gross, C., Kneissl, T., Bishop, J. L., Roush, T. L., and McKay, C. P. Evidence for hesperian impact-induced hydrothermalism on mars. *Icarus*, 208(2):667 – 683, 2010. ISSN 0019-1035. doi: https://doi.org/10.1016/j.icarus.2010.03.013. URL http://www.sciencedirect.com/science/article/pii/S0019103510001156.

McLennan, S. M., Bell, J. F., Calvin, W. M., Christensen, P. R., Clark, B. C., de Souza, P. A., Farmer, J., Farrand, W. H., Fike, D. A., Gellert, R., Ghosh, A., Glotch, T. D., Grotzinger, J. P., Hahn, B., Herkenhoff, K. E., Hurowitz, J. A., Johnson, J. R., Johnson, S. S., Jolliff, B., Klingelhöfer, G., Knoll, A. H., Learner, Z., Malin, M. C., McSween, H. Y., Pocock, J., Ruff, S. W., Soderblom, L. A., Squyres, S. W., Tosca, N. J., Watters, W. A., Wyatt, M. B., and Yen, A. Provenance and diagenesis of the evaporite-bearing burns formation, meridiani planum, mars. *Earth and Planetary Science Letters*, 240(1):95–121, 2005. doi: https://doi.org/10.1016/j.epsl.2005.09.041. URL http://www.sciencedirect.com/science/article/pii/S0012821X05006357.

McMillan, P. F., Lees, V., Quirico, E., Montagnac, G., Sella, A., Reynard, B., Simon, P.,

Bailey, E., Deifallah, M., and Corà, F. Graphitic carbon nitride C6N9H3·HCl: Characterisation by UV and near-IR FT Raman spectroscopy. *Journal of Solid State Chemistry*, 182 (10):2670–2677, 2009. ISSN 0022-4596. doi: https://doi.org/10.1016/j.jssc.2009.07.030. URL http://www.sciencedirect.com/science/article/pii/S0022459609003363.

Meyers, P. A. and Ishiwatari, R. Lacustrine organic geochemistry—an overview of indicators of organic matter sources and diagenesis in lake sediments. *Organic Geochemistry*, 20(7): 867 – 900, 1993. ISSN 0146-6380. doi: https://doi.org/10.1016/0146-6380(93)90100-P. URL http://www.sciencedirect.com/science/article/pii/014663809390100P.

Mignon, P., Corbin, G., Le Crom, S., Marry, V., Hao, J., and Daniel, I. Adsorption of nucleotides on clay surfaces. Effects of mineral composition, pH and solution salts. *Applied Clay Science journal*, 2019. submitted.

Montagnac, G., Cardon, H., Daniel, I., and Reynard, B. Structural changes in perylene from UV Raman spectroscopy up to 1 GPa. *Journal of Raman Spectroscopy*, 47(6):720–725, 2016. doi: 10.1002/jrs.4890. URL https://onlinelibrary.wiley.com/doi/abs/10.1002/jrs.4890.

Paineau, E., Bihannic, I., Baravian, C., Philippe, A.-M., Davidson, P., Levitz, P., Funari, S. S., Rochas, C., and Michot, L. J. Aqueous suspensions of natural swelling clay minerals. 1. structure and electrostatic interactions. *Langmuir*, 27(9):5562–5573, 2011. doi: 10.1021/la2001255. URL https://doi.org/10.1021/la2001255.

Patel, M., Zarnecki, J., and Catling, D. Ultraviolet radiation on the surface of Mars and the Beagle 2 UV sensor. *Planetary and Space Science*, 50(9):915 – 927, 2002. ISSN 0032-0633. doi: https://doi.org/10.1016/S0032-0633(02)00067-3. URL http://www.sciencedirect.com/science/article/pii/S0032063302000673. Space Related Laboratory Investigation: Materials, environments a nd life.

Patel, M., Bérces, A., Kolb, C., Lammer, H., Rettberg, P., Zarnecki, J., and Selsis, F. Seasonal and diurnal variations in Martian surface ultraviolet irradiation: Biological and chemical implications for the Martian regolith. *International Journal of Astrobiology*, 2(1):21–34, 2003. doi: 10.1017/S1473550402001180.

Pedreira-Segade, U., Feuillie, C., Pelletier, M., Michot, L. J., and Daniel, I. Adsorption of nucleotides onto ferromagnesian phyllosilicates: Significance for the origin of life. *Geochimica et Cosmochimica Acta*, 176:81 – 95, 2016. ISSN 0016-7037. doi: https://doi.org/10.1016/j.gca.2015.12.025. URL http://www.sciencedirect.com/science/article/pii/S001670371500719X.

Pedreira-Segade, U., Hao, J., Razafitianamaharavo, A., Pelletier, M., Marry, V., Le Crom, S., Michot, L. J., and Daniel, I. How do nucleotides adsorb onto clays? *Life*, 8(4), 2018a. ISSN 2075-1729. doi: 10.3390/life8040059. URL http://www.mdpi.com/2075-1729/8/4/59.

Pedreira-Segade, U., Michot, L. J., and Daniel, I. Effects of salinity on the adsorption of nucleotides onto phyllosilicates. *Phys. Chem. Chem. Phys.*, 20:1938–1952, 2018b. doi: 10.1039/C7CP07004G. URL http://dx.doi.org/10.1039/C7CP07004G.

Poch, O., Jaber, M., Stalport, F., Nowak, S., Georgelin, T., Lambert, J.-F., Szopa, C., and Coll, P. Effect of nontronite smectite clay on the chemical evolution of several organic molecules under simulated Martian surface ultraviolet radiation conditions. *Astrobiology*, 15(3):221–237, 2015. doi: 10.1089/ast.2014.1230. PMID: 25734356.

Poulet, F., Bibring, J.-P., Mustard, J. F., Gendrin, A., Mangold, N., Langevin, Y., Arvidson, R. E., Gondet, B., Gomez, C., Berthé, M., Bibring, J.-P., Langevin, Y., Erard, S., Forni, O., Gendrin, A., Gondet, B., Manaud, N., Poulet, F., Poulleau, G., Soufflot, A., Combes, M., Drossart, P., Encrenaz, T., Fouchet, T., Melchiorri, R., Bellucci, G., Altieri, F., Formisano, V., Fonti, S., Capaccioni, F., Cerroni, P., Coradini, A., Korablev, O., Kottsov, V., Ignatiev, N., Titov, D., Zasova, L., Mangold, N., Pinet, P., Schmitt, B., Sotin, C., Hauber, E., Hoffmann, H., Jaumann, R., Keller, U., Arvidson, R., Mustard, J., Forget, F., and Team, T. O. Phyllosilicates on Mars and implications for early Martian climate. *Nature*, 438(7068):623–627, 2005. ISSN 1476-4687. URL https://doi.org/10.1038/nature04274.

Quirico, E., Montagnac, G., Lees, V., McMillan, P. F., Szopa, C., Cernogora, G., Rouzaud, J.-N., Simon, P., Bernard, J.-M., Coll, P., Fray, N., Minard, R. D., Raulin, F., Reynard, B., and Schmitt, B. New experimental constraints on the composition and structure of tholins. *Icarus*, 198, Issue 1:218, 2008.

Russell, M. P., Vohník, S., and Thomas, J., G J. Design and performance of an ultraviolet resonance Raman spectrometer for proteins and nucleic acids. *Biophysical journal*, 68(7787047):1607–1612, 1995. ISSN 1542-0086. URL https://www.ncbi.nlm.nih.gov/pmc/articles/PMC1282056/.

Sapers, H. M., Razzell Hollis, J., Bhartia, R., Beegle, L. W., Orphan, V. J., and Amend, J. P. The cell and the sum of its parts: Patterns of complexity in biosignatures as revealed by deep UV Raman spectroscopy. *Frontiers in Microbiology*, 10:679, 2019. ISSN 1664-302X. doi: 10.3389/fmicb.2019.00679. URL https://www.frontiersin.org/article/10.3389/fmicb.2019.00679.

561 Shkolyar, S., Eshelman, E. J., Farmer, J. D., Hamilton, D., Daly, M. G., and Youngbull, C. Detecting kerogen
562 as a biosignature using colocated UV time-gated Raman and fluorescence spectroscopy. *Astrobiology*, 18(4):
563 431–453, 2018. doi: 10.1089/ast.2017.1716. PMID: 29624103.

564 Steele, A., Benning, L. G., Wirth, R., Siljeström, S., Fries, M. D., Hauri, E., Conrad, P. G., Rogers, K., Eigen-
565 brode, J., Schreiber, A., Needham, A., Wang, J. H., McCubbin, F. M., Kilcoyne, D., and Rodriguez Blanco,
566 J. D. Organic synthesis on Mars by electrochemical reduction of CO2. *Science Advances*, 4(10), 2018. doi:
567 10.1126/sciadv.aat5118. URL https://advances.sciencemag.org/content/4/10/eaat5118.

568 Toyama, A., Ohta, K., and Takeuchi, H. Correlation between the UV resonance Raman in-
569 tensity and hydrogen bonding of the adenine ring. *Journal of Molecular Structure*, 735-736:
570 235 – 241, 2005. ISSN 0022-2860. doi: https://doi.org/10.1016/j.molstruc.2004.11.004. URL
571 http://www.sciencedirect.com/science/article/pii/S0022286004008671.

572 Wadsworth, J. and Cockell, C. S. Perchlorates on Mars enhance the bacteriocidal effects of UV light. *Scientific*
573 *Reports*, 7(1):4662, 2017. ISSN 2045-2322. URL https://doi.org/10.1038/s41598-017-04910-3.

574 Wang, L., Tuschel, D., and Asher, S. A. 229 nm UV photochemical degradation of energetic molecules. In III,
575 A. W. F. and Gardner, P. J., editors, *Chemical, Biological, Radiological, Nuclear, and Explosives (CBRNE)*
576 *Sensing XII*, volume 8018, pages 367 – 372. International Society for Optics and Photonics, SPIE, 2011. doi:
577 10.1117/12.887061. URL https://doi.org/10.1117/12.887061.

578 Williford, K. H., Farley, K. A., Stack, K. M., Allwood, A. C., Beaty, D., Beegle, L. W., Bhartia, R., Brown,
579 A. J., de la Torre Juarez, M., Hamran, S.-E., Hecht, M. H., Hurowitz, J. A., Rodriguez-Manfredi, J. A.,
580 Maurice, S., Milkovich, S., and Wiens, R. C. Chapter 11 - The NASA Mars 2020 rover mission and the search
581 for extraterrestrial life. In Cabrol, N. A. and Grin, E. A., editors, *From Habitability to Life on Mars*, pages
582 275–308. Elsevier, 2018. ISBN 978-0-12-809935-3. doi: https://doi.org/10.1016/B978-0-12-809935-3.00010-4.
583 URL http://www.sciencedirect.com/science/article/pii/B9780128099353000104.

mode	wavenumber (cm^{-1})	vibration
ν_1	900-1200	PO_4 degenerate stretching mode
ν_2	1325	Imidazole ring stretching localized around N7
ν_3	1360	C2=N3-C4-N9 stretching mode
ν_4	1490	C2=N3 C4=C5 N7=C8 extending across both rings
ν_5	1570	Pyrimidine stretching mode involving N3
ν_6	1605	Pyrimidine ring mode and/or NH_2 scissor

Table 1: Strong modes observed in resonant Raman spectra of dGMP dry films. The attribution of Raman modes is from previous studies (Ghomi and Taillandier, 1985; Fodor et al., 1985; Russell et al., 1995; Lee et al., 2017).

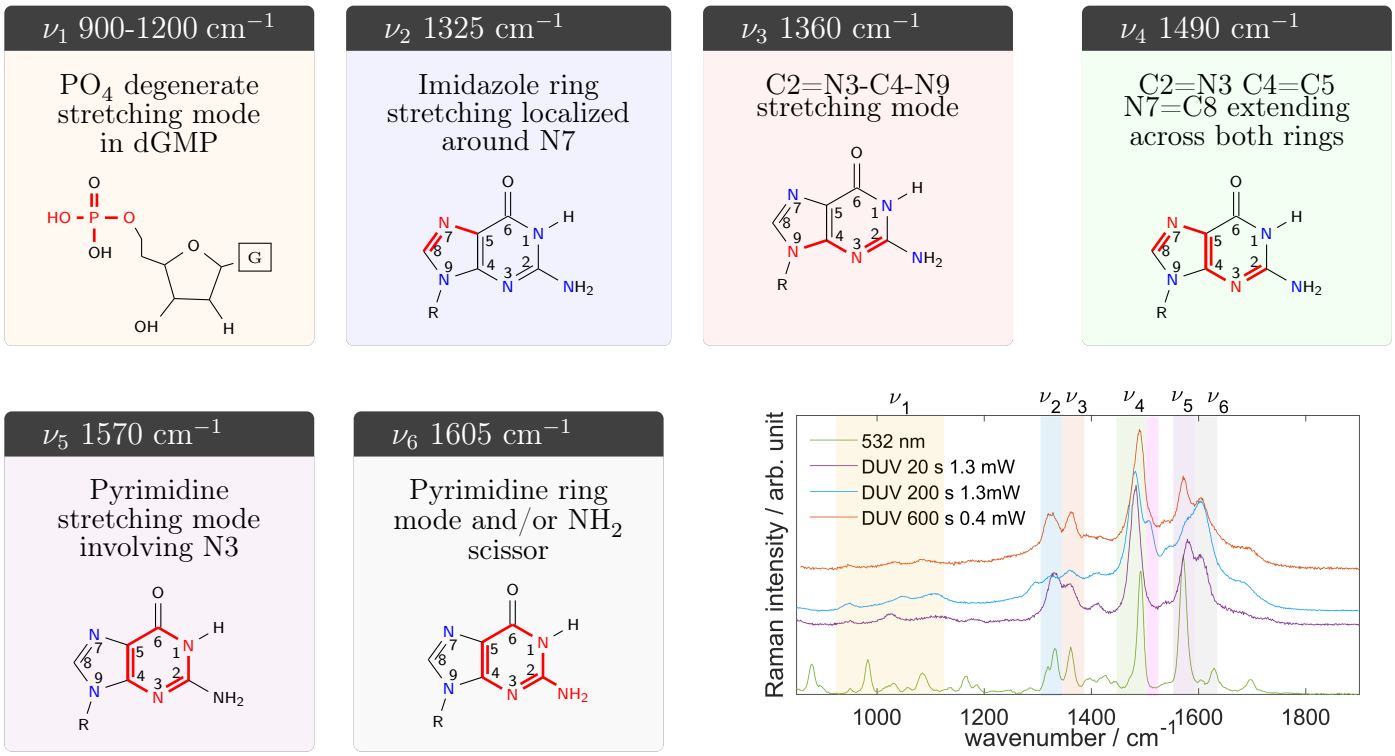

Figure 1: Peak positions of the DUV-RR modes of dGMP and their assignments according to present and previous results (Fodor et al., 1985; Russell et al., 1995; Lee et al., 2017). Panels sketch intense vibrational modes highlighted in red in the nucleotide structure and indicate the corresponding wavenumber in the header of the box. They are color coded, and stripes with the same color superimposed to Raman spectra in all figures to highlight these vibrational modes. Bottom right: the Raman spectrum of a concentrated dGMP solution excited with 532 nm wavelength is compared to DUV-RR spectra of a dry dGMP film measured with a 244 nm excitation.

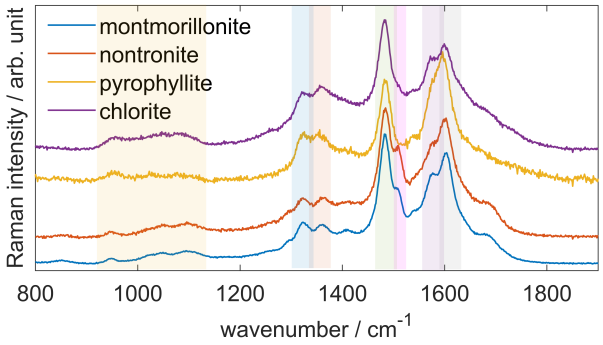

Figure 2: DUV-RR spectra of 10 mM of dGMP adsorbed onto some clay minerals and phyllosilicates, namely, montmorillonite, nontronite, pyrophyllite and chlorite. The in-plane vibrations of the purine (pyrimidine-imidazole) heterocycle are color-coded as in the panels of Figure 1.

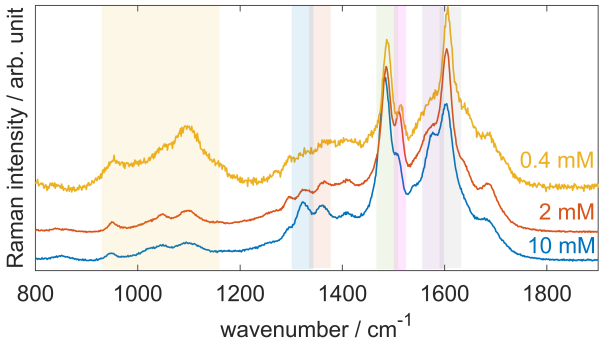

Figure 3: DUV-RR spectra of adsorbed dGMP with different concentrations 0.4, 2 and 10 mM on montmorillonite. Same color-code as in Figure 1.

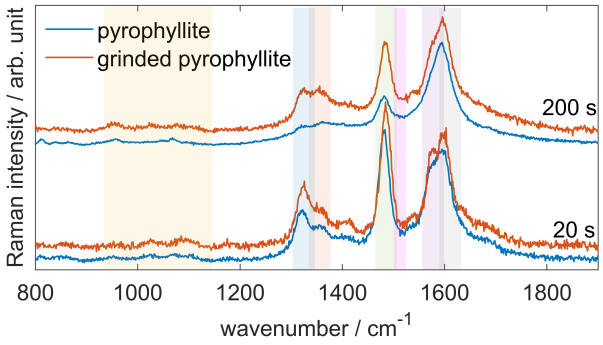

Figure 4: DUV-RR spectra of adsorbed dGMP onto pyrophyllite powder. Spectra in blue and red correspond to minerals with different grain size of 10 and 1 µm or less, respectively. Same color-code as in Figure 1.

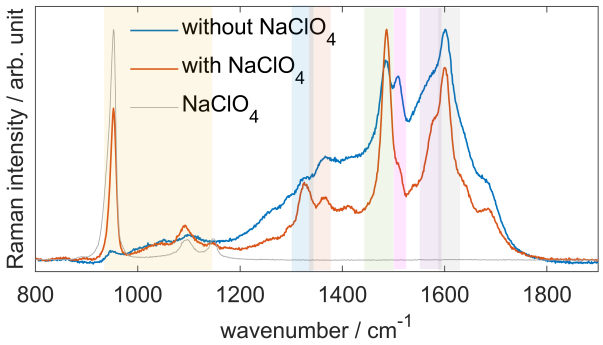

Figure 5: DUV-RR spectra of $NaClO_4$ perchlorate deposit (grey), dGMP+perchlorate+montmorillonite (red) and dGMP+montmorillonite (blue). dGMP is diluted in perchlorate solution at 4 mM of concentration and adsorbed onto montmorillonite. The spectra are corrected with a linear baseline and normalized to the maximum intensity. Same color-code as in Figure 1.

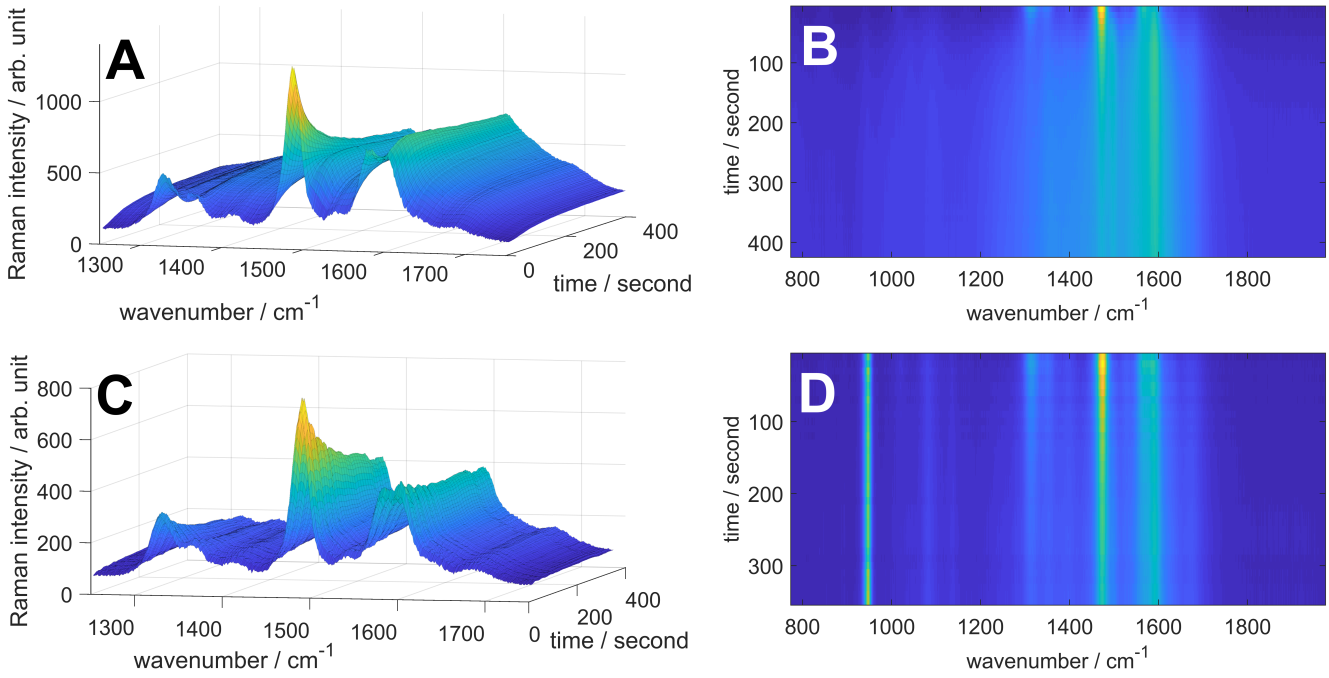

Figure 6: Evolution of DUV-RR spectra of dGMP adsorbed onto montmorillonite mineral as a function of time up to 400 seconds under the UV laser beam. Left column figures are surface images from acquisition sequences of 10 seconds time lapse. Right column figures are 2D time lapse of the Raman intensities. A and B are without $NaClO_4$ perchlorate, C and D are with perchlorate.